Unidirectional transmission in photonic-crystal gratings at beam-type illumination

Atilla Ozgur Cakmak,[1,*] Evrim Colak,[1] Andriy E. Serebryannikov,[2] and Ekmel Ozbay[1]

[1]*Nanotechnology Research Center, Department of Physics, Department of Electrical and Electronics Engineering, Bilkent University, 06800 Ankara, Turkey*
[2]*Hamburg University of Technology, E-3, D-21071 Hamburg, Germany*
**atilla@ee.bilkent.edu.tr*

Abstract: Unidirectional transmission is studied theoretically and experimentally for the gratings with one-side corrugations (non-symmetric gratings), which are based on two-dimensional photonic crystals composed of alumina rods. The unidirectional transmission appears at a fixed angle of incidence as a combined effect of the peculiar dispersion features of the photonic crystal and the properly designed corrugations. It is shown that the basic unidirectional transmission characteristics, which are observed at a plane-wave illumination, are preserved at Gaussian-beam and horn antenna illuminations. The main attention is paid to the single-beam unidirectional regime, which is associated with the strong directional selectivity arising due to the first negative diffraction order. An additional degree of freedom for controlling the transmission of the electromagnetic waves is obtained by making use of the asymmetric corrugations at the photonic crystal interface.

OCIS codes: (230.5298) Photonic crystals; (050.7330) Volume gratings; (260.1960) Diffraction theory; (120.7000) Transmission; (260.2110) Electromagnetic optics.

References and links

1. Z. Wang, Y. D. Chong, J. D. Joannopoulos, and M. Soljacić, "Reflection-free one-way edge modes in a gyromagnetic photonic crystal," Phys. Rev. Lett. **100**(1), 013905 (2008).
2. F. D. M. Haldane, and S. Raghu, "Possible realization of directional optical waveguides in photonic crystals with broken time-reversal symmetry," Phys. Rev. Lett. **100**(1), 013904 (2008).
3. Z. Yu, Z. Wang, and S. Fan, "One-way total reflection with one-dimensional magneto-optical photonic crystals," Appl. Phys. Lett. **90**(12), 121133 (2007).
4. M. Scalora, J. P. Dowling, C. M. Bowden, and M. J. Bloemer, "The photonic band edge optical diode," J. Appl. Phys. **76**(4), 2023 (1994).
5. A. Figotin, and I. Vitebskiy, "Electromagnetic unidirectionality and frozen modes in magnetic photonic crystals," J. Magn. Magn. Mater. **300**(1), 117–121 (2006).
6. A. Figotin, and I. Vitebskiy, "Electromagnetic unidirectionality in magnetic photonic crystals," Phys. Rev. B **67**(16), 165210 (2003).
7. A. E. Serebryannikov, "One-way diffraction effects in photonic crystal gratings made of isotropic materials," Phys. Rev. B **80**(15), 155117 (2009).
8. B. T. Schwartz, and R. Piestun, "Total external reflection from metamaterials with ultralow refractive index," J. Opt. Soc. Am. B **20**(12), 2448 (2003).
9. A. E. Serebryannikov, and E. Ozbay, "Unidirectional transmission in non-symmetric gratings containing metallic layers," Opt. Express **17**(16), 13335–13345 (2009).
10. A. E. Serebryannikov, and E. Ozbay, "Isolation and one-way effects in diffraction on dielectric gratings with plasmonic inserts," Opt. Express **17**(1), 278–292 (2009).
11. M. J. Lockyear, A. P. Hibbins, K. R. White, and J. R. Sambles, "One-way diffraction grating," Phys. Rev. E Stat. Nonlin. Soft Matter Phys. **74**(5), 056611 (2006).
12. W.-M. Ye, X.-D. Yuan, C.-C. Guo, and C. Zen, "Unidirectional transmission in non-symmetric gratings made of isotropic material," Opt. Express **18**(8), 7590–7595 (2010).
13. N. Bonod, E. Popov, L. Li, and B. Chernov, "Unidirectional excitation of surface plasmons by slanted gratings," Opt. Express **15**(18), 11427–11432 (2007).
14. I. P. Radko, S. I. Bozhevolnyi, G. Brucoli, L. Martín-Moreno, F. J. García-Vidal, and A. Boltasseva, "Efficient unidirectional ridge excitation of surface plasmons," Opt. Express **17**(9), 7228–7232 (2009).
15. S. Cakmakyapan, A. E. Serebryannikov, H. Caglayan, and E. Ozbay, "One-way transmission through the subwavelength slit in nonsymmetric metallic gratings," Opt. Lett. **35**(15), 2597–2599 (2010).
16. R. Petit, *Electromagnetic theory of gratings* (Springer, Berlin, 1980).

#133429 - $15.00 USD Received 16 Aug 2010; revised 23 Sep 2010; accepted 27 Sep 2010; published 6 Oct 2010

17. R. Moussa, S. Foteinopoulou, L. Zhang, G. Tuttle, K. Guven, E. Ozbay, and C. M. Soukoulis, "Negative refraction and superlens behavior in a two-dimensional photonic crystal," Phys. Rev. B **71**(8), 085106 (2005).
18. C. Luo, S. G. Johnson, J. D. Joannopoulos, and J. B. Pendry, "All-angle negative refraction without negative effective index," Phys. Rev. B **65**(20), 201104 (2002).

1. Introduction

Realization of various functions in the optical and microwave frequency ranges leads to the demand in the devices with strong directional selectivity. In the limiting case of the directional selectivity such a device would allow (nearly) total transmission in one direction and no transmission in the opposite direction within the same propagation channel, which can be considered as the electromagnetic counterpart of a diode. The conventional approach to achieve the unidirectional transmission in passive devices is based on the use of the anisotropic [1–3] or nonlinear [4] materials. In particular, the strongly pronounced unidirectional transmission has been demonstrated for the one-dimensional photonic crystals (PCs) [5,6] and for the stacks of the two-dimensional PCs [1], in which anisotropic materials were utilized. Directional waveguides have been realized in PCs with broken time-reversal symmetry [2].

In the last years, the interest has been directed towards the potential of the structures, which are made of purely isotropic materials, in achieving strong directional selectivity. This directional selectivity might be similar, but not exactly the same as those achievable due to the anisotropy. In particular, it has been demonstrated that at a fixed angle of incidence most part of the energy of the incident plane wave can be transmitted from half space 1 to half space 2, while no transmission occurs from half space 2 to half space 1, provided that a PC grating is located in between so that the interface bounding half space 1 is only corrugated [7]. The transmission mechanism studied therein is based on exploiting the dispersion features of the PCs, which facilitate that the zero (reciprocal) order is not coupled to a Floquet-Bloch wave of the PC at a proper choice of the angle of incidence, while several higher diffraction orders may exist due to the effect of corrugations and may be coupled as long as the grating is illuminated from the side of corrugations.

The unidirectional transmission can be obtained for different types of dispersion of the PCs, which also include that corresponding to the ultralow-index media [8]. Therefore, it is not surprising to observe that the same unidirectional effect can be obtained in purely metallic non-symmetric gratings, as well as in the gratings comprising dielectric and metallic layers [9]. When we compare the results presented in [7,9–11], it can be inferred that the unidirectional transmission is also obtainable for the metallic slabs with the periodic branched slits at non-zero angles of incidence, which have been studied at normal incidence in [11]. Hence, the effect of the unidirectional transmission in non-symmetric gratings is rather general and can be obtained for various grating performances, provided that the corrugations, the dispersion, and the angle of incidence are properly chosen. In addition to the above-mentioned structures, the unidirectional transmission may appear, for example, in non-symmetric gratings based on one- and three-dimensional PCs. The unidirectional transmission can also be achieved in the specially designed combination of the two dielectric gratings, which enable the dramatic reduction of the contribution of the zero order [12]. Moreover, the asymmetric excitation of the surface plasmons on the metallic corrugated surfaces has been studied in [13,14]. Recently, another mechanism for the unidirectional transmission has been suggested, which is based on the excitation of the surface plasmons on the corrugated surfaces of the non-symmetric metallic gratings with a single slit [15].

In this paper, we investigate the directional selectivity in the PC gratings in the microwave regime at beam-type illumination. In contrast to our earlier theoretical studies of the higher-order related unidirectional transmission, in which the consideration had been restricted to the plane-wave illumination, we focus on the validation of this mechanism for Gaussian-beam and horn antenna illuminations in the present study. The geometry of the gratings is similar to one of those studied in [7], but shows some differences in the shape and depth of the corrugations. The simulations and the microwave experiments are performed for a wide frequency range that involves the first five PC bands (Floquet-Bloch waves), which are

#133429 - $15.00 USD Received 16 Aug 2010; revised 23 Sep 2010; accepted 27 Sep 2010; published 6 Oct 2010

distinguished in terms of their respective dispersion features. The presented results include the transmission spectra of the examined structures for the plane-wave illumination, the frequency response of the transmittance for Gaussian-beam and horn antenna illuminations, and the angular distributions of the transmittance, at a proper value of the angle of incidence.

2. Grating geometry and experimental setup

The PC grating has been designed by taking into account our previous experience with such structures, availability of the materials, and the existing experimental facilities. Since the studied mechanism is relatively new, it is worth while performing the first experiments by using horn antennas at the microwave frequencies. It is expected to be scalable down to much smaller frequencies. For the purposes of comparison, simulations for the Gaussian-beam and the plane-wave illuminations have been scaled to match the same frequency range. We decided in favor of the performance that is based on the square-lattice PC composed of alumina rods with a relative permittivity ε = 9.61 and a diameter d = 3.1mm. The lattice constant is a = 7mm. The grating is assembled as an 8x100 array. Some of the cells were left empty by removing the rods at specific locations in order to obtain the corrugations at one of the interfaces.

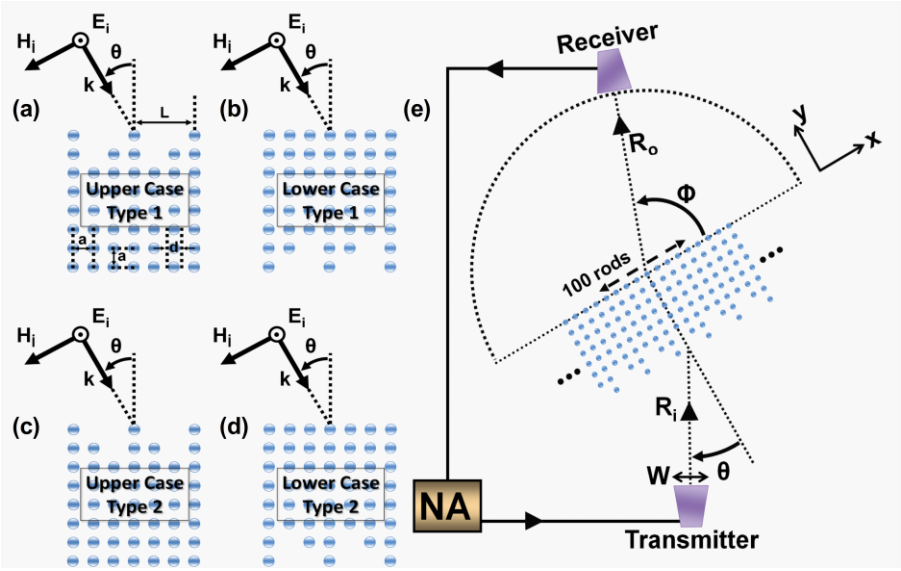

Fig. 1. The geometry of the PC grating under study (two lateral periods are shown) – illustrations (a)-(d) and the schematic of the experimental setup – illustration (e). NA stands for the Network Analyzer, W represents the aperture size of the horn antenna.

Figures 1(a)–1(d) schematically show the cases that will be studied in this paper. Contrary to the PC gratings considered in [7], for which the grating period was $L = 4a$, here we take $L = 3a$. A reduction in the grating period assures obtaining a desired strong directional selectivity at smaller values of kL (k is the free-space wavenumber) while illuminating a smaller area of the input interface. Furthermore, the corrugations in Fig. 1 are placed asymmetrically with respect to the interface normal, which is also distinguished from the PC gratings studied in [7]. The grating that is seen from the side of the interface is associated with a *structured echelette*. Its asymmetry with respect to the interface normal offers two transmission regimes by switching between the two orientations of the interface "triangle", which can be handled by changing the sign of the incidence angle.

The experimental setup is schematically shown in Fig. 1(e). It contains an Agilent two-port 8510C Network Analyzer, and two standard pyramidal horn antennas with an operational frequency range starting from 16 GHz up to 30 GHz. The distances R_i = 20cm and R_0 = 1m were used in the experiment. In this case, the input (illuminated) interface of the grating is

#133429 - $15.00 USD Received 16 Aug 2010; revised 23 Sep 2010; accepted 27 Sep 2010; published 6 Oct 2010

located in the near zone of the transmitter antenna, while the incident wavefronts possess a significant curvature and the angular plane-wave spectrum of the incident wave is relatively wide. In fact, the transmitter antenna can be considered as a model of an optical source with a moderate directivity. Our study is restricted to the case when the electric field vector is parallel to the rod axes.

For the sake of definiteness, we refer to the PC interface without echelette-type corrugations as the non-corrugated interface throughout the paper. In turn, the interface showing such corrugations is referred to as the corrugated interface. Strictly speaking, the non-corrugated interface represents itself as a periodic structure with a period of a. However, the non-zero diffraction orders may appear in this case at $ka>\pi$, which corresponds to $kL>3\pi$ and, hence, this range is beyond our main interest. At intermediate values of the angle of incidence (θ), which are expected to be the most appropriate for obtaining a single-beam unidirectional transmission, the higher orders can be generated by the non-corrugated interface starting from even larger values of kL (e.g. at $kL>4\pi$ for $\theta<60^{o}$), so that the suggested terminology is quite reasonable for most of the considered cases.

3. Simulation results for plane-wave illumination

First of all, the plane-wave transmission has been studied in order to justify the choice of the geometrical and the material parameters of the gratings in Fig. 1, and to provide a connection to the results obtained for the PC gratings in [7]. According to the general theory of diffraction gratings [16], transmittance is determined as follows:

$$T = \sum_{M}^{N} t_n, \tag{1}$$

where t_n is n^{th} order partial transmittance, and M and N are the smallest and the largest indices of the propagating orders, respectively. Throughout the paper, the transmittance is denoted with $T^{\rightarrow}$ for the cases when the corrugated interface is illuminated (upper cases in Fig. 1), and the notation $T^{\leftarrow}$ is used for the cases when the non-corrugated interface is illuminated (lower cases in Fig. 1). For all of the finite-thickness diffraction gratings, $t_0^{\rightarrow} = t_0^{\leftarrow}$ (reciprocal component) and $t_n^{\rightarrow} \neq t_n^{\leftarrow}$ (non-reciprocal components), if θ = const, $M \le n \le N$, and $n \neq 0$. At some special frequency values, the situation can be realized such that $t_n^{\rightarrow} = t_n^{\leftarrow}$ at $n \neq 0$. For the PC gratings [7] and the gratings containing metallic layers [9], the non-reciprocity of the non-zero (higher) orders can manifest itself so that $t_n^{\rightarrow} \neq 0$ but $t_n^{\leftarrow} = 0$ within a wide frequency range, while θ is kept constant. Therefore, if the zero order is not coupled to a Floquet-Bloch wave of the PC, the unidirectional transmission may be obtained, i.e., simultaneously $T^{\rightarrow} \neq 0$ and $T^{\leftarrow} = 0$, for a wide frequency range.

According to [7,9], a non-zero θ is required for obtaining a single-beam unidirectional transmission. Figure 2 presents an example of the transmission spectra which are characterized by relatively large values of $T^{\rightarrow} \neq 0$ over relatively wide bandwidths. Five kL-ranges can be spotted in Fig. 2, where $T^{\rightarrow} \neq 0$ and $T^{\leftarrow} \approx 0$. They are centered nearly at kL = 4.9, 8.1, 9.6, 11.8, and 14.1, i.e., for all of them $ka<2\pi$. Consequently, they can be labeled as the unidirectional passbands. The bandwidths of the regarding passbands are 3.5%, 4.1%, 7.8%, 18.2%, and 11.3%, respectively. Then, we have a single-beam unidirectional transmission $T^{\rightarrow} = t_{-1}$ except for the third lowest range. Based on the obtained results, we select the ranges of variation of kL, which are particularly interesting for the experimental study. The ranges which will be studied in detail are denoted by A, B, and C in Fig. 2. Among them, only the ranges A and C correspond to the single-beam transmission. The range denoted by * is narrower than the range A, and it is characterized by smaller values of $T^{\rightarrow}$. Besides, the transmittance is weaker in the range denoted by # than in the range C. Moreover, the operational frequency range of our horn antennas for the specified PC parameters is most

#133429 - $15.00 USD Received 16 Aug 2010; revised 23 Sep 2010; accepted 27 Sep 2010; published 6 Oct 2010

suitable for the ranges A, B and C, which mainly relates our main scope to these unidirectional bands.

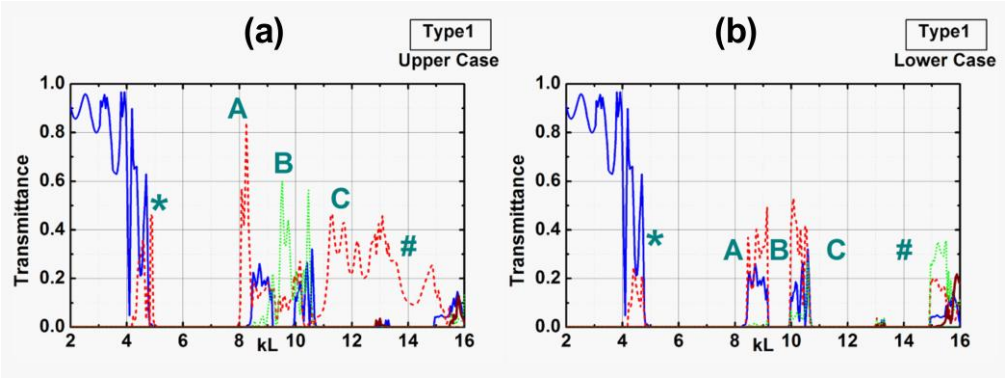

Fig. 2. The transmittance for the cases shown in Fig. 1(a) – plot (a) and Fig. 1(b) – plot (b); solid blue line – zero order, dashed thicker red line – first negative order, dotted green line – second negative order, solid wine-colored line – first positive order; $\theta = 30^{o}$.

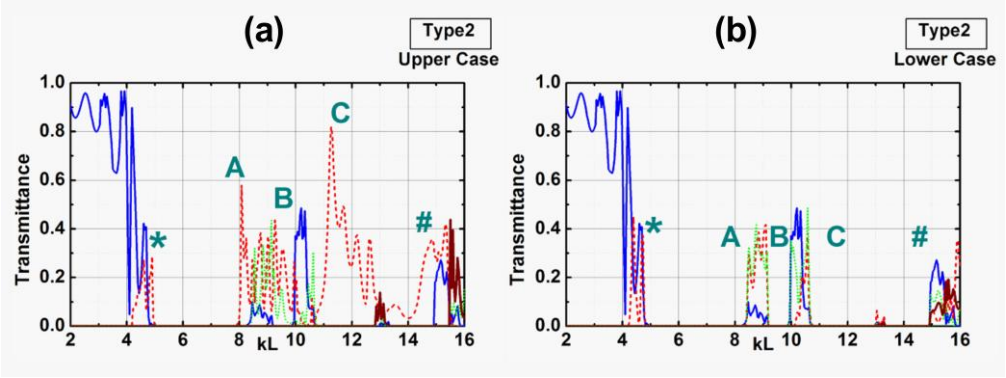

Fig. 3. Same as in Fig. 2 but for the cases shown in Fig. 1(c) – plot (a), and Fig. 1(d) – plot (b).

In Fig. 3, the transmission spectra are shown at the same parameters as in Fig. 2, but the difference is that now the other side of the interface "triangle" is illuminated. It is seen that changing the illumination in such a way can result in a significant modification of the transmission within the ranges A, B and C, but does not lead to new unidirectional passbands. In particular, the maximal value of $T^{\rightarrow} = 0.82$ is obtained inside the range C at kL = 11.26. This value is comparable with those obtained earlier for the two-dimensional PC gratings [7] and the special combination of the two dielectric gratings [12]. The location and, hence, the width of the unidirectional passbands are slightly different as compared to Fig. 2 owing to the different strengths of the diffraction and the different contributions of the individual diffraction orders. The results presented in Figs. 2 and 3 are obtained by using an integral equation method.

Figure 4 presents the isofrequency dispersion contours (IFCs) for the corresponding infinite PC with periods $a_x = a_y = a$, at several typical values of kL taken from for the ranges A and C. The horizontal dashed lines are assumed to be parallel to the non-corrugated interface. The signs "+" and "–" at the top depicts whether a diffraction order is coupled to a Floquet-Bloch wave or not in the upper case as in Figs. 1(a) and 1(c). On the other hand, the signs "–" and "X" at the bottom signify whether a diffraction order is not coupled to a Floquet-Bloch wave, or cannot exist at all in the lower case as in Figs. 1(b) and 1(d).

#133429 - $15.00 USD Received 16 Aug 2010; revised 23 Sep 2010; accepted 27 Sep 2010; published 6 Oct 2010

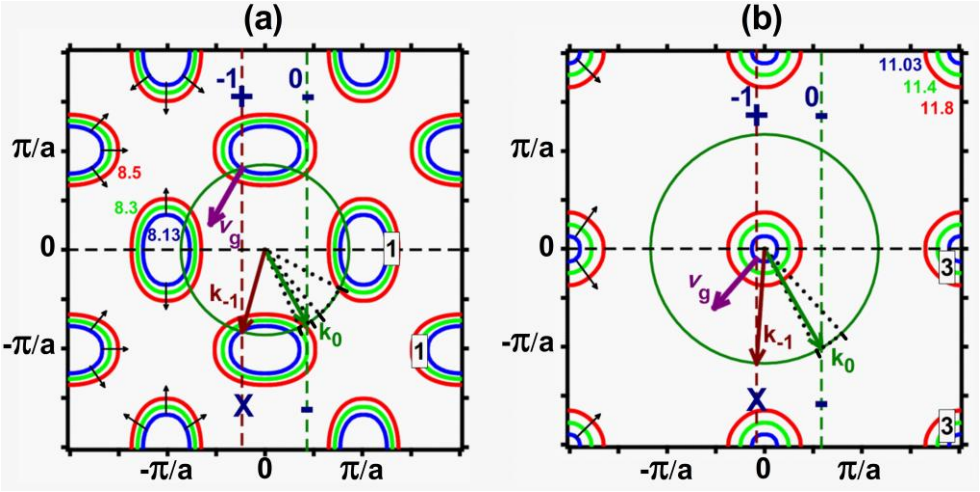

Fig. 4. IFCs of the PC on the (k_x,k_y)-plane in the vicinity of kL = 8.3 – plot (a), and in the vicinity of kL = 11.4 – plot (b). The numbers of the PC bands (Floquet-Bloch wave numbers start from 0) are shown in the boxes. Thin arrows show the possible directions of the gradients that indicate the directions of the group velocity, v_g. The air IFCs (green circles), the construction lines (vertical dashed lines), the wave vectors of the diffraction orders, k_0 and k_{-1} (intermediately thick arrows) and the directions of v_g (thick arrows) correspond to kL = 8.13 in plot (a) and kL = 11.03 in plot (b). The vectors k_0 and k_{-1} and the directions of v_g are shown here at θ = 30° and at the illumination direction depicted in Figs. 1(a) and 1(c). The dotted lines show the ranges of k_0, where the unidirectional transmission is expected to appear.

In Fig. 4(a), the dispersion is non-isotropic with the IFCs located around X point ($k_x = \pi/a$, $k_y = 0$) of the irreducible Brillouin zone. Then, the zero order is not coupled if

$$k_{\min}^{(2)} > k_{\|} > k_{\max}^{(1)}, \qquad (2)$$

where $k_{\|}$ is the tangential component of the incident wave vector, $k_{\max}^{(1)}$ and $k_{\min}^{(2)}$ are the maximal k_x for the IFCs near $k_x = 0$ and the minimal k_x for the IFCs near $k_x = \pi/a$, provided that $k_{\|} > 0$. At kL = 8.13, Eq. (2) is satisfied nearly within the range 24°<θ<63°. In this range, $t_{-1}^{\rightarrow}$ may be non zero. Moreover, only the first negative order is coupled to a Floquet-Bloch wave at 24°<θ<33° and 40°<θ<63°, while the first and second negative orders both contribute to the transmission at 33°≤θ≤40°. In Fig. 4(b), the dispersion is nearly isotropic with 0<n_{eff}<1, i.e., the IFC for the PC is centralized around Γ point ($k_x = k_y = 0$) and it is narrower than the IFC for air. In particular, n_{eff} = 0.11 at kL = 11.03. In this case, Eq. (2) is satisfied already at θ>27°, while $k_{\min}^{(2)}$ is formally equal here to $2\pi/a - k_{\max}^{(1)}$. However, the range of θ where $t_{-1}^{\rightarrow} \neq 0$ and $t_{-1}^{\leftarrow} = 0$ is much narrower, because the IFC is very narrow. Here, it occurs within the range 27°<θ<47°.

Therefore, regardless of the differences in the IFC shape, the zero order cannot be coupled to a Floquet-Bloch wave at θ = 30°. If the first negative order may exist in this case due to the shape of the input interface, it is the only coupled order in the upper case at kL = 8.13 and kL = 11.03. This is also true for the other kL values from the ranges A and C. The negative refraction is mimicked at the input interface in Fig. 4 by the only coupled order, i.e. by the first negative order, since $\mathrm{sgn}(\mathbf{v_g}\cdot\hat{x}) \neq \mathrm{sgn}(\mathbf{k_0}\cdot\hat{x})$. It is interesting that in contrast to the PCs with non-corrugated interfaces, e.g., see [17,18], the negative refraction can be achieved in the presently studied PC gratings not only without a left handedness, but also with a positive effective index of refraction, as seen in Fig. 4(b). Furthermore, the single outgoing beam must be negatively deflected because $\mathrm{sgn}(\mathbf{k_0}\cdot\hat{x}) \neq \mathrm{sgn}(\mathbf{k_{-1}}\cdot\hat{x})$. On the other hand, neither the

#133429 - $15.00 USD Received 16 Aug 2010; revised 23 Sep 2010; accepted 27 Sep 2010; published 6 Oct 2010

negative refraction at the input interface nor the negative deflection of the transmitted beam appear when only the zero order is coupled, as it occurs for small positive θ. Note that the IFCs in Fig. 4 are analogous to those in Figs. 3 and 13 in [7], where they are presented for a PC with similar parameters. In turn, the IFCs for the range B (not shown here) are similar to those in Fig. 7 in [7]. In this case, they are nearly flat and located around Γ and M points, where M point corresponds to $k_x = k_y = \pi/a$. Furthermore, in accordance with our earlier claims concerning Figs. 2 and 3, the second negative order is also coupled together with the first negative order in range B. Thus, we do not observe a single-beam unidirectional transmission regime around these kL values at $\theta = 30°$.

4. Simulation results for Gaussian-beam illumination

The Gaussian-beam illumination is considered in this section, which is in some sense an intermediate step between a plane-wave and a horn antenna illumination. We utilize a Gaussian beam with a width of $10a$, whose source is located $R_i = 20$cm away from the input interface, while the transmittance is calculated at a distance $R_0 = 1$m away from the output interface, see Fig. 1(e). For the chosen beam width and distances, the plane-wave nature of the incident wavefronts is still strongly pronounced. Nevertheless, we should still take into account the effect coming from the finite-width angular plane-wave spectrum of the incident Gaussian beam, which implies the contribution of the other angular components associated with an angle different from θ.

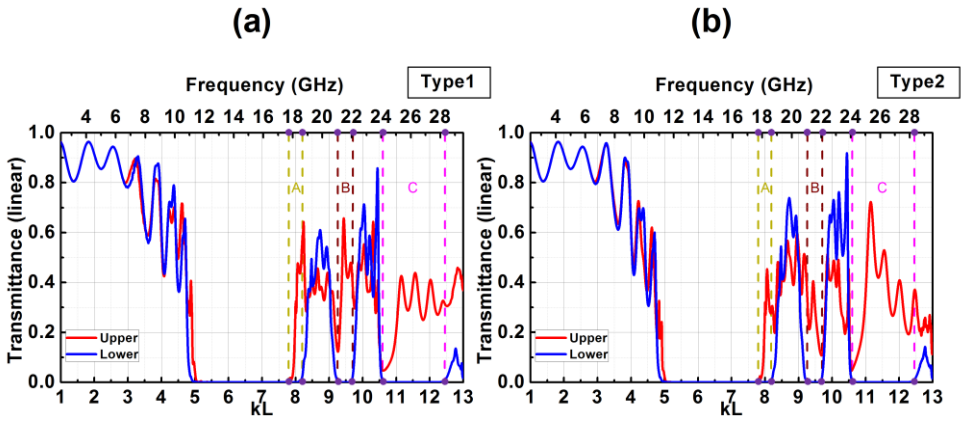

Fig. 5. The integral transmittance at the Gaussian-beam illumination: left plot corresponds to Figs. 1(a) and 1(b), right plot corresponds to Figs. 1(c) and 1(d); solid blue line - the illumination is from the non-corrugated interface (Lower), red line – the illumination is from the corrugated interface (Upper); $\theta = 30°$.

An FDTD code has been used for the simulations. In Fig. 5, the integral transmittances, $\tau^{\rightarrow}$ and $\tau^{\leftarrow}$ are presented as a function of kL for all four cases from Figs. 1(a)–1(d). They are calculated as follows:

$$\tau^{\rightarrow} = \frac{1}{\pi}\int_0^{\pi} T^{\rightarrow}(\Phi)d\Phi, \quad \text{and} \quad \tau^{\leftarrow} = \frac{1}{\pi}\int_0^{\pi} T^{\leftarrow}(\Phi)d\Phi. \tag{3}$$

In fact, if $\tau^{\rightarrow}$ (red lines) and $\tau^{\leftarrow}$ (blue lines) are calculated in the far zone, they represent analogs of $T^{\rightarrow}$ and $T^{\leftarrow}$ at a beam-type illumination. In contrast with Figs. 2 and 3, the contribution of the individual orders cannot be specified here. However, the basic features are the same in Figs. 2, 3 and 5. The ranges of the unidirectional transmission, A, B, and C, are centered now nearly at $kL = 8$, 9.46, and 11.5 in both Fig. 5(a) and Fig. 5(b), i.e., they show nearly the same locations as the plane-wave illumination in Figs. 2 and 3 suggests.

#133429 - $15.00 USD Received 16 Aug 2010; revised 23 Sep 2010; accepted 27 Sep 2010; published 6 Oct 2010

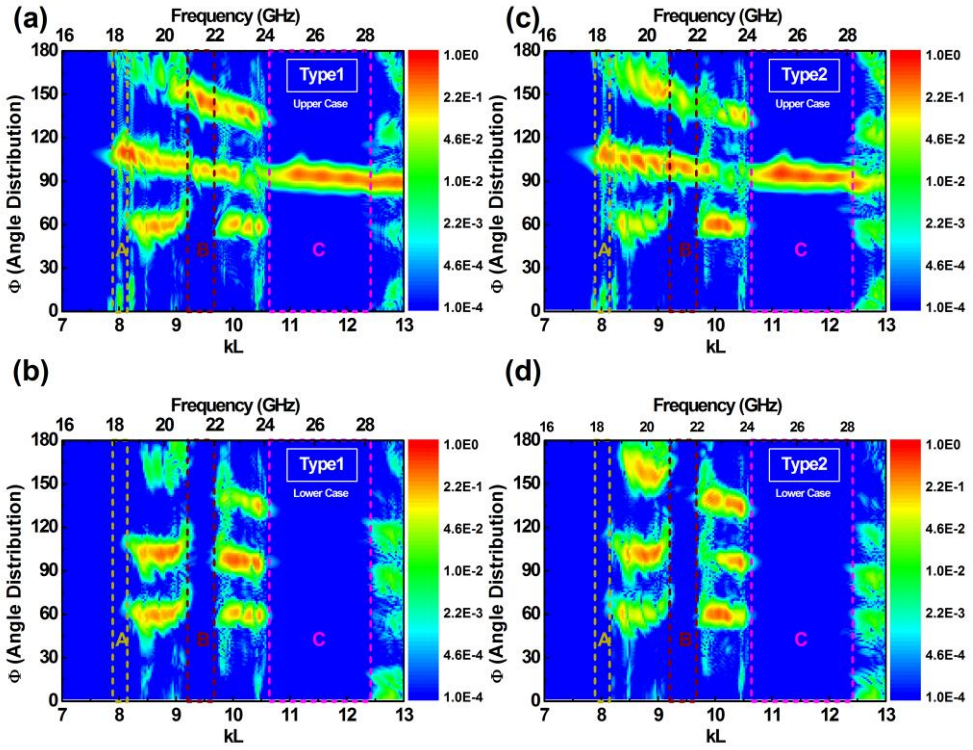

Fig. 6. Transmittance (in logarithmic scale) at the Gaussian-beam illumination on (kL,Φ)-plane: plots (a), (b), (c) and (d) correspond to Figs. 1(a), 1(b), 1(c) and 1(d), respectively; $\theta = 30^{\circ}$.

Figure 6 presents $T^{\rightarrow}$ and $T^{\leftarrow}$ on the (kL,Φ)-plane, at the same Gaussian-beam illumination as in Fig. 5. Here, Φ is the observation angle that is defined in Fig. 1. This type of a presentation of the results allows us to associate the basic transmission features with the contribution of the individual diffraction orders. One can immediately distinguish the areas where the transmission is strong in the upper case but very weak in the lower case by comparing Fig. 6(a) with Fig. 6(b) and Fig. 6(c) with Fig. 6(d). These areas are located inside the ranges A, B, and C, which are bounded here at the same kL values as in Fig. 5. The angle of diffraction of the n^{th} order in the transmission half-space is determined from the following equation:

$$\phi_n = \sin^{-1}(\sin\theta + 2\pi n / kL). \qquad (4)$$

The diffraction angle, ϕ_n in Eq. (4) is measured in the clockwise direction from the y-axis, it is connected to the observation angle, Φ, as $\phi_n = -\Phi + \pi/2$. Then, one can easily see that the lowest-Φ areas of significant transmission in Fig. 6 should be associated with the zero order ($\Phi = 60^{\circ}$ corresponds to $\phi_n = 30^{\circ}$). In turn, the middle ($85^{\circ}<\Phi<120^{\circ}$) and the most upper ($\Phi>130^{\circ}$) areas correspond to the first-negative-order and the second-negative-order transmission. Although the boundary between the areas of the strong and weak transmission is blurred, the appearance of the strong directional selectivity is well demonstrated. In Fig. 6, the range C seems to be the most promising candidate for the experimental verification of the unidirectional transmission not only because it is wider than the ranges A and B, but also because of the better isolation from the weaker transmission coming from the adjacent areas. Note that the absolute transmission values are depicted in Fig. 6. A pulse function in the time domain has been employed as the source in order to attain the transmission values over a wide frequency range. The monitored intensity values that are collected 1m away from the exit side of the PC are normalized with respect to the free space transmission results for each kL value,

#133429 - $15.00 USD Received 16 Aug 2010; revised 23 Sep 2010; accepted 27 Sep 2010; published 6 Oct 2010

and thereby the problem originating from the inefficiency of the pulse function to excite a relatively wide frequency range in a balanced manner is overcome.

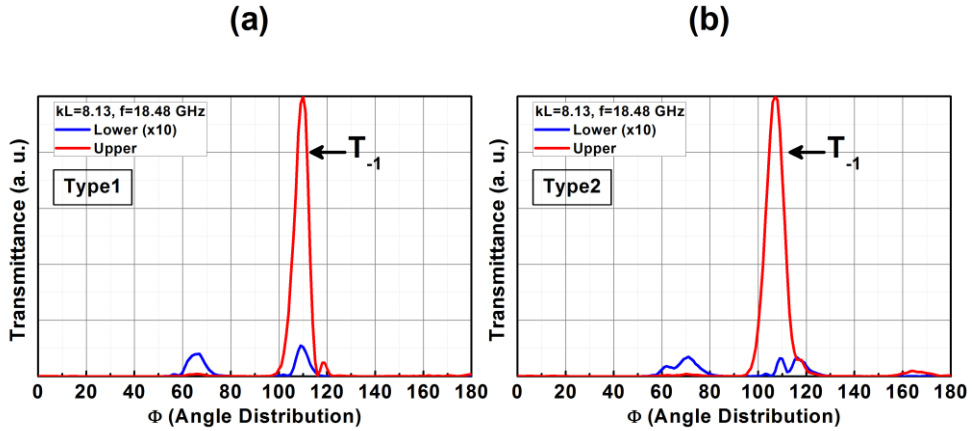

Fig. 7. Angular dependence of the transmittance at a frequency value from the range A: plot (a) corresponds to Figs. 1(a) and 1(b), plot (b) corresponds to Figs. 1(c) and 1(d); blue line – the non-corrugated interface is illuminated, red line – the corrugated interface is illuminated; R_i = 20cm; $\theta = 30^o$.

Figure 7 presents T vs Φ, which has been calculated at a selected frequency value that is taken from the range A. The strong contrast between the forward and backward transmittance is well seen by comparing the blue and red lines. Next, we focus our attention to the location of the peaks of T. It is noteworthy that a peak arising at $\Phi = \pi/2$ would correspond to $\phi_n = 0$, i.e., to the case when the n^{th}-order transmitted beam propagates along the y-axis so that $\mathbf{k_n} \cdot \hat{x} = 0$. At least at large distances away from the grating, the cases of $\phi_n>0$ and $\phi_n<0$ correspond to the transmitted beams with $\mathbf{k_n} \cdot \hat{x} > 0$ and $\mathbf{k_n} \cdot \hat{x} < 0$, respectively. Furthermore, a significant lateral beam shift can appear at the output interface. If $\Phi-\pi/2 + \phi_n>0$, the negative shift should manifest itself in angular location of the maximum of T. If $\Phi-\pi/2 + \phi_n<0$, the positive shift takes place. According to Eq. (4), $\phi_{-1} = -15.8°$. In turn, at the maxima of T in Figs. 7(a) and 7(b), we obtain $\Phi = 110°$ and $\Phi = 107°$, respectively. Hence, the angular deviation for the beam-type illumination turns out to be $\zeta_{-1} = \Phi-\pi/2 + \phi_{-1} = 4.2°$ in Fig. 7(a) and $\zeta_{-1} = 1.2°$ in Fig. 7(b). The observed negative shift qualitatively coincides with the predictions based on the wave vector diagram in Fig. 4(a). The effect of the corrugation shape and the orientation of the interface on the value of ζ_{-1} and on the lateral shift at the output interface will be studied in a forthcoming paper.

In Fig. 8, the angular distribution is presented at the same kL-value from the range C, for which the wave vector diagram was plotted in Fig. 4(b). Here, $\phi_{-1}\approx-4°$, so that the outgoing beam should propagate in the direction that is nearly normal to the output interface. In turn, $\Phi = 95°$ and $\zeta_{-1}\approx1°$ in both Fig. 8(a) and Fig. 8(b). Thus, the obtained results are in qualitative agreement with the wave vector diagram. In this case, both the mimicking of the negative refraction at the input interface and the negative deflection of the transmitted beam take place. Moreover, the transmission contrast is very strong. In particular, at the maximum of $T^{\rightarrow}$ (red line), we obtain $T^{\rightarrow}/T^{\leftarrow} = 1.75\times10^4$ in Fig. 8(a) and $T^{\rightarrow}/T^{\leftarrow} = 2.07\times10^4$ in Fig. 8(b).

#133429 - $15.00 USD Received 16 Aug 2010; revised 23 Sep 2010; accepted 27 Sep 2010; published 6 Oct 2010

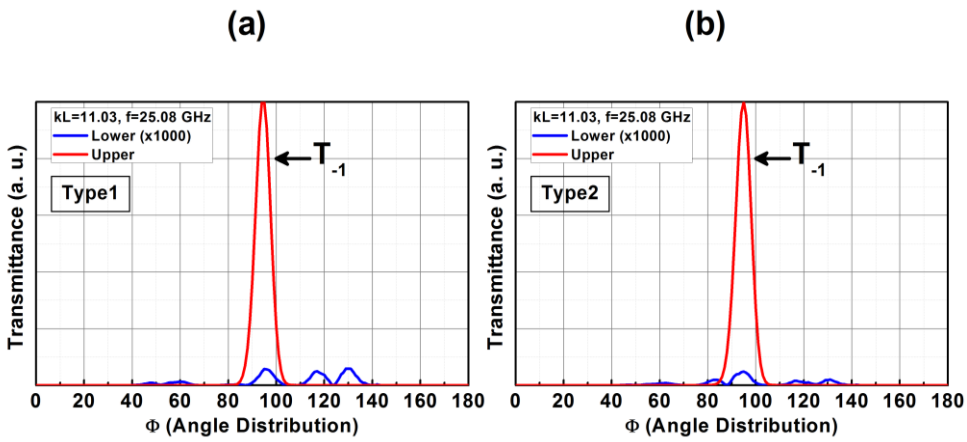

Fig. 8. Same as Fig. 7 but for a frequency value taken from the range C.

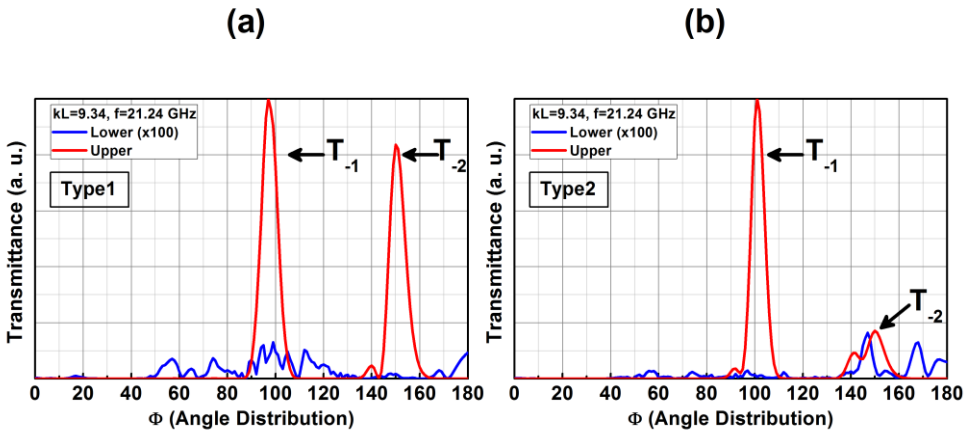

Fig. 9. Same as Fig. 7 but for a frequency value taken from the range B.

For the comparison, Fig. 9 shows the angular distribution for the *kL*-value taken from the range B. Here, in contrast to Figs. 7 and 8, two higher orders are coupled to a Floquet-Bloch wave at the input (corrugated) interface, and thus two beams appear in the transmission. According to Eq. (4), $\phi_{-1} = -9.95°$ and $\phi_{-2} = -57.7°$. In turn, from the simulation results, we obtain $\Phi = 97°$ and $\Phi = 150°$ for the first and second peaks of T shown by the red line in Fig. 9(a), and $\Phi = 101°$ and $\Phi = 150°$ for the first and second peaks of T shown by red line in Fig. 9(b). Correspondingly, $T^{\rightarrow}/T^{\leftarrow} = 1.34\times10^{3}$ and $T^{\rightarrow}/T^{\leftarrow} = 5.42\times10^{3}$ for the first and second peaks in Fig. 9(a), and $T^{\rightarrow}/T^{\leftarrow} = 1.43\times10^{4}$ and $T^{\rightarrow}/T^{\leftarrow} = 192$ for the first and second peaks in Fig. 9(b). The extent to which the second negative order contributes to the transmission can be varied due to changing the sign of θ. It is noteworthy that the first negative order corresponds to the square-like IFC located around Γ point, while the second negative order corresponds to the square-like IFC surrounding M point.

5. Experimental results for horn antenna illumination

The first series of the measurements have been performed while placing the transmitter antenna at a distance R_i = 25cm away from the input interface, and the receiver antenna at the

#133429 - $15.00 USD Received 16 Aug 2010; revised 23 Sep 2010; accepted 27 Sep 2010; published 6 Oct 2010

distance R_o = 1m away from the output interface. The effect of the incident wave's angular spectrum width is expected to be more prominent in the case of the horn antenna illumination than in the Gaussian-beam illumination case. In addition, the curvature of the wavefronts that reach the PC interface still keeps the strong non-planar features. The results are presented in Fig. 10 on the (kL,Φ)-plane for the ranges A and C. Here and in the other similar figures, the dashed lines approximately show the areas, within which the transmission is significant only for the upper case.

The unidirectional transmission can be clearly seen from the comparison of Fig. 10(a) with Fig. 10(b), and Fig. 10(c) with Fig. 10(d). The same advantages of the range C are recognized here as for the Gaussian-beam illumination, i.e., weak transmittance in adjacent larger and smaller Φ ranges, larger bandwidth, and stronger contrast between the upper case and the lower case. The transmission results were calibrated with respect to the free space measurements.

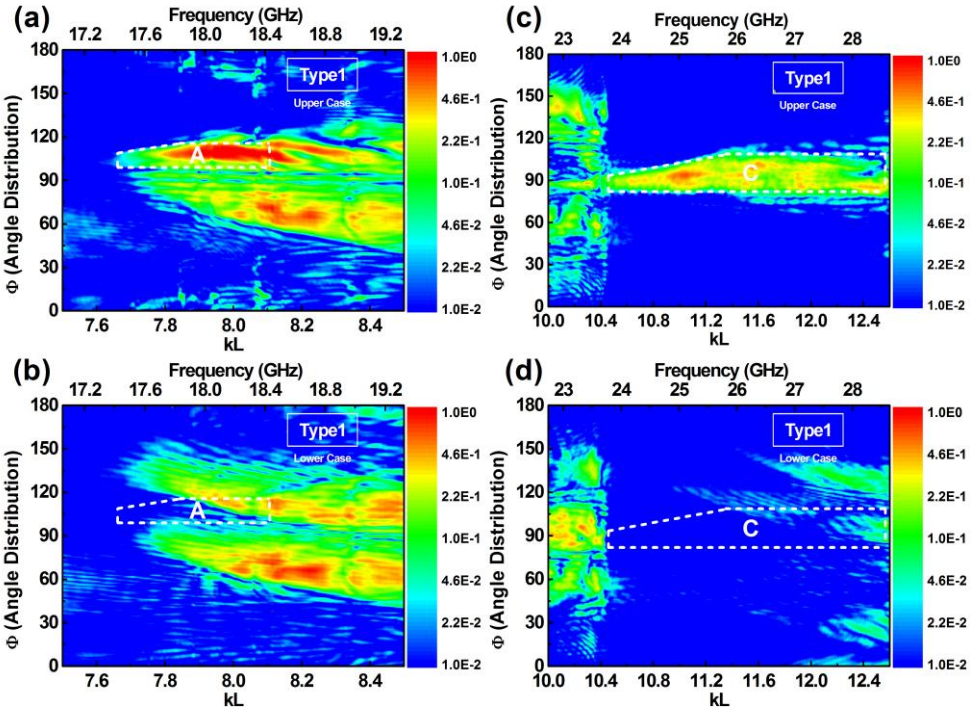

Fig. 10. The measured transmittance (in arbitrary units, in logarithmic scale) on the (kL,Φ)-plane for the range A in the upper case as in Fig. 1(a) – plot (a), for the range A in the lower case in Fig. 1(b) – plot (b), for the range C in the upper case as in Fig. 1(a) – plot (c), and for the range C in the lower case as in Fig. 1(b) – plot (d); R_i = 25cm.

The locations of the areas shown by the dashed lines quite well coincide with the predictions, which are based on the dispersion results and the transmission results for the plane-wave and Gaussian-beam illuminations. In particular, the corner points of the mentioned areas correspond to Φ = 98° and Φ = 110° at f = 17.4 GHz, and to Φ = 98° and Φ = 116° at f = 18.43 GHz in Figs. 10 (a) and 10(b), respectively. In Figs. 10(c) and 10(d), the corner points correspond to Φ = 80° and Φ = 93° at f = 23.78 GHz, and Φ = 80° and Φ = 109° at f = 28.6 GHz. The contrast $T^{\rightarrow}/T^{\leftarrow}$ exceeds 200 for the transmission data in Figs. 10(a) and 10 (b) and 900 for those in Figs. 10(c) and 10(d).

Figure 11 presents the measured transmittance maps, which differ from those in Figs. 10(c) and 10(d) in that now the input (corrugated) interface is illuminated from the other

#133429 - $15.00 USD Received 16 Aug 2010; revised 23 Sep 2010; accepted 27 Sep 2010; published 6 Oct 2010

side of the interface "triangles". Here, the uppermost and lowest points of the ellipse that is shown by the dashed line correspond to $\Phi = 116°$ and $\Phi = 74°$, respectively, while $f = 25.89$ GHz. The leftmost and rightmost points correspond to $f = 23.84$ GHz and $f = 27.95$ GHz while $\Phi = 95°$. The maximal contrast for the data in Fig. 11 is nearly the same as for those in Fig. 10. Based on the plane-wave and Gaussian-beam results obtained for the range C, one could expect a stronger transmission in the upper case in the vicinity of $kL = 11$ for Type 2 than for Type 1. Indeed, from the comparison of Fig. 10(c) with Fig. 11(a), one can see that this feature is preserved at the horn antenna illumination, too.

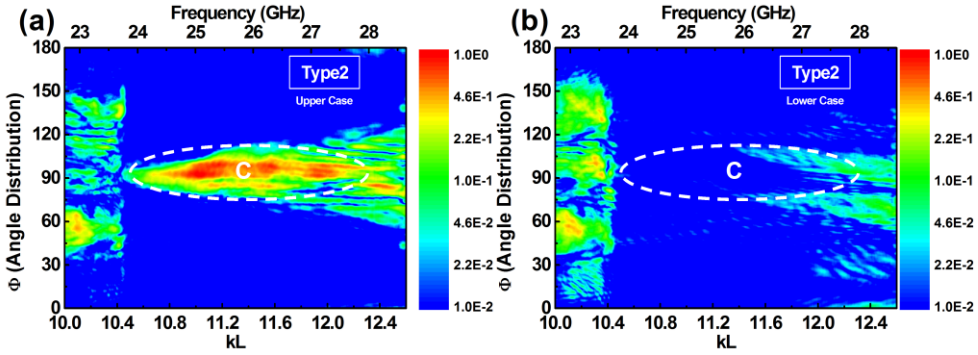

Fig. 11. The measured transmittance (in arbitrary units, in logarithmic scale) on the (kL,Φ)-plane for the range C in the upper case as in Fig. 1(c) – plot (a), and for the range C in the lower case as in Fig. 1(d) – plot (b); $R_i = 25$cm.

The second series of the experiments have been carried out by placing the transmitter antenna further away from the grating, i.e., at $R_i = 60$cm while $R_o = 1$m is kept. The main goal was to estimate the extent, to which the above-discussed features could be modified, and detect the factors, which might be dominant for such a modification. Among such factors, one should mention the possible diffraction at the grating edges, variations in the angular plane-wave spectrum of the incident wave, and the curvature of the incident wavefronts that varies with the distance from the input interface. An example is presented in Fig. 12. The basic features remain the same, but significant transmission appears now within those areas where it was typically near-zero for $R_i = 25$cm. In particular, relatively weak but not negligible transmission appears within rather wide ranges that are in the vicinity of $\Phi = 60°$ at $f<17.6$ GHz in Figs. 12(a) and 12(b), and at 24 GHz$<f<$27 GHz in Figs. 12(c) and 12(d). One could deduce that the effect of the zero order is pronounced here by comparing the values of Φ with those of $\pi/2$-ϕ_0, and also by judging the fact that these ranges appear in both the lower case and the upper case. This might indicate, in particular, that the angular spectrum of the incident wave become wider for a larger R_i, so that the contribution of the spectral components, which correspond to the plane waves incident at the angles that allow coupling of the zero order to a Floquet-Bloch wave, become more significant.

#133429 - $15.00 USD Received 16 Aug 2010; revised 23 Sep 2010; accepted 27 Sep 2010; published 6 Oct 2010

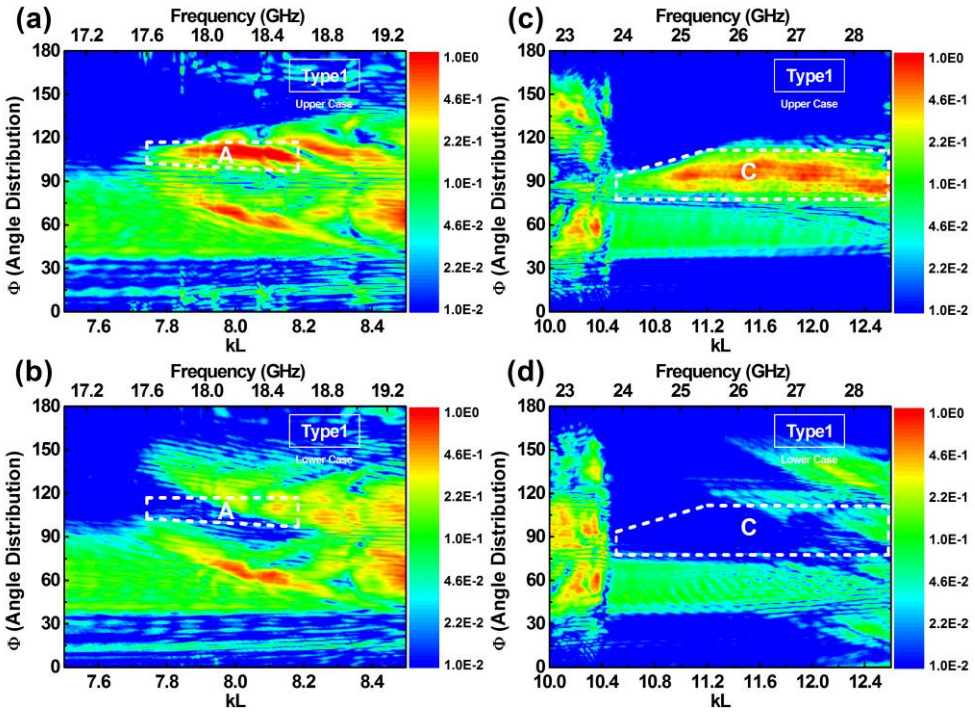

Fig. 12. Same as Fig. 10 but for R_i = 60cm.

In Figs. 12(a) and 12(b), the corner points of the area bounded by the dashed line are located at Φ = 100° and Φ = 117° for f = 17.6 GHz, and at Φ = 95° and Φ = 117° for f = 18.6 GHz. In Figs. 12(c) and 12(d), they are located at Φ = 77° and Φ = 100° for f = 23.84 GHz, and at Φ = 77° and Φ = 112° for f = 28.66 GHz. In other words, they show nearly the same locations as in Figs. 10(a)-10(d). In fact, now we have a *combination of two-way and one-way transmission regions* for both A and C ranges. Despite this, the transmission contrast for the areas bounded by the dashed line remains within the same range of variation as in Figs. 10 and 11.

Figure 13 presents the experimental variation of $\tau^{\rightarrow}$ (red lines) and $\tau^{\leftarrow}$ (blue lines) as a function of kL, which correspond to Figs. 10(c), 10(d), 11(a), and 11(b). The presented results differ from those in Fig. 5 only in the type of the incident wave. Although the one-way transmission in Fig. 13 is weaker pronounced, and the boundaries of the corresponding kL-range are blurred, the same basic features can be recognized. In particular, we again observe (i) a maximum of transmission in the vicinity of kL = 11, (ii) a stronger transmission for Type 2 than for Type 1, and (iii) a strong local minimum of transmission in the vicinity of kL = 10.5 in Fig. 13(b) [compare with Figs. 5(a) and 5(b)].

#133429 - $15.00 USD Received 16 Aug 2010; revised 23 Sep 2010; accepted 27 Sep 2010; published 6 Oct 2010

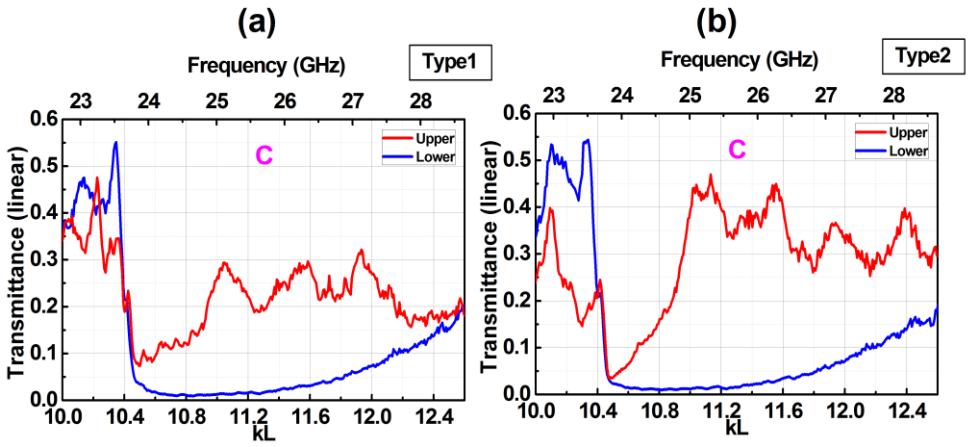

Fig. 13. The integral transmittance in the kL range, which includes the range C: plot (a) corresponds to Figs. 1(a) and 1(b), plot (b) corresponds to Figs. 1(c) and 1(d); R_i = 25cm.

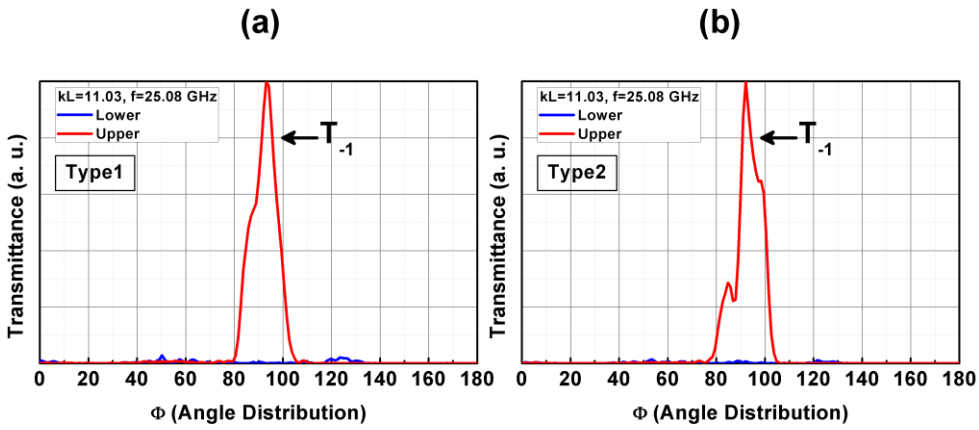

Fig. 14. The measured angular distribution of the transmittance for a kL value taken from the range C: plot (a) corresponds to Figs. 1(a) and 1(b), plot (b) corresponds to Figs. 1(c) and 1(d); R_i = 25cm.

The measured angular distributions of $T^{\rightarrow}$ and $T^{\leftarrow}$ are presented at kL = 11.03 (range C) in Fig. 14. The maxima of $T^{\rightarrow}$ occurs at Φ = 93° in Fig. 14(a) and at Φ = 92° in Fig. 14(b). These values are in good coincidence with those in Figs. 8(a) and 8(b), and also with the corresponding value of $\phi_1 \approx -4°$. The contrast at the peaks is 2.98×10^3 in Fig. 14(a) and 850 in Fig. 14(b). Hence, the transmittance can be vanishing for all Φ values in the lower case also at horn antenna illumination, at least if R_i is relatively small.

It has been observed in Figs. 10 and 12 that non-negligible two-way transmittance can start to appear at Φ<90° at those values of kL for which it was negligibly small at R_i = 25cm, as we increase R_i. An example of the manifestation of this effect in the angular dependence at a fixed kL is presented in Fig. 15. It is mainly associated with the zero order, since Φ = 60° corresponds to ϕ_0 = 30° and $t_0^{\rightarrow} = t_0^{\leftarrow}$ at the plane-wave illumination. Here, it appears nearly at 35°<Φ<80°. At the same time, the strong one-way transmission remains within the range of variation of Φ, which is associated with the first negative order. The maxima are located here

#133429 - $15.00 USD Received 16 Aug 2010; revised 23 Sep 2010; accepted 27 Sep 2010; published 6 Oct 2010

at Φ = 95° in Fig. 15(a) and at Φ = 93° in Fig. 15(b), respectively. These values are in good coincidence with those in Fig. 14 and with the value of $\phi_1 \approx -4°$. The contrast is equal to 730 at the maximum in Fig. 15(a) and 1.04×10^3 at the maximum in Fig. 15(b). In fact, this regime is similar to the one studied for the metallic slabs with the branched slits [11]. Indeed, we obtain nearly reciprocal transmission within one range of the Φ variation, and simultaneously the strongly pronounced unidirectional transmission within another range of the Φ variation.

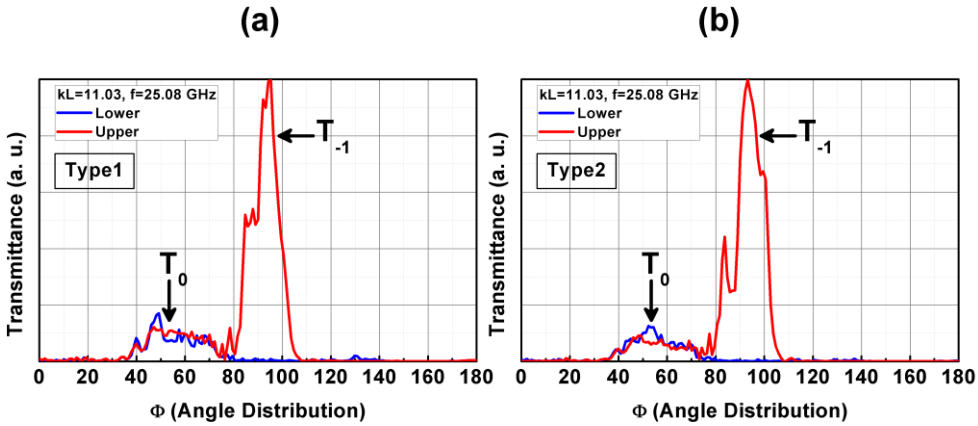

Fig. 15. Same as Fig. 14 but for R_i = 60cm.

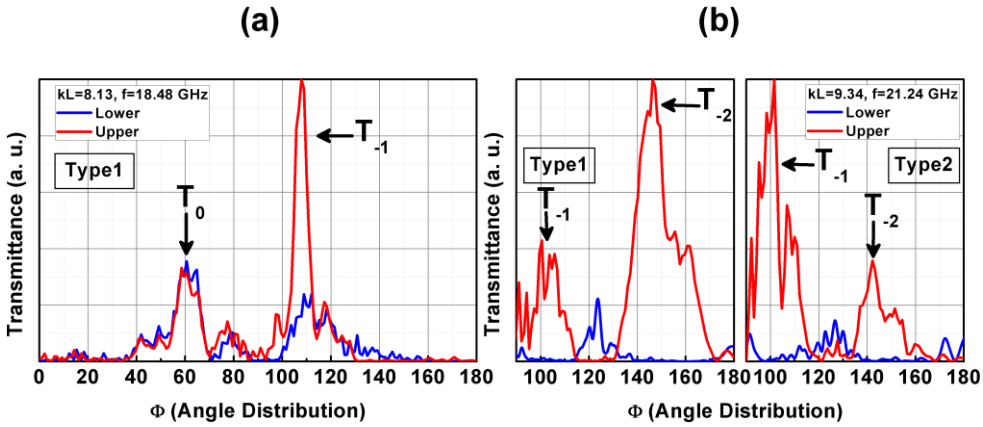

Fig. 16. The measured angular distribution of the transmittance for *kL* values taken from the range A – plot (a), and range B – plot (b); plot (a) and left panel of plot (b) correspond to Figs. 1(a) and 1(b), right panel in plot (b) corresponds to Figs. 1(c) and 1(d); R_i = 60cm.

Finally, let us check whether the strong directional selectivity remains at R_i = 60cm in the ranges A and B. Figure 16 presents the measured transmittance for the same values of *kL* as in Figs. 7 and 9. In Fig. 16(a), the maximal transmittance is observed at Φ = 107°. It is associated with the first negative order since $\pi/2-\phi_1$ = 105.8°. However, the one-way transmission that is pronounced here is much weaker than in Fig. 15. At the maximum, we obtain $T^{\rightarrow}/T^{\leftarrow} = 5.6$. Furthermore, the transmission associated with the zero order is stronger compared to Fig. 15. As a result, $T^{\leftarrow} = 0$ cannot be obtained, at least for those values of Φ where $T^{\rightarrow}$ takes large

#133429 - $15.00 USD Received 16 Aug 2010; revised 23 Sep 2010; accepted 27 Sep 2010; published 6 Oct 2010

values. It is noteworthy that the zero-order related maximum appears in the upper case at Φ = 59° while $\pi/2-\phi_{-1}$ = 60°.

In Fig. 16(b), one can see that although $T^{\leftarrow}$ cannot vanish in the lower case for all values of Φ, strong directional selectivity remains within particular Φ-ranges, which are associated with the first and second negative orders. The corresponding maxima appear at Φ = 100.5° and Φ = 146.3° in the left panel in Fig. 16(b), and at Φ = 101.5° and Φ = 142° in the right panel in Fig. 16(b), while $\pi/2-\phi_{-1}$ = 100° and $\pi/2-\phi_{-2}$ = 147.7°. The contrasts are $T^{\rightarrow}/T^{\leftarrow}=44$ and $T^{\rightarrow}/T^{\leftarrow}=140$ for the maxima associated with the first and second negative orders in the left panel, and $T^{\rightarrow}/T^{\leftarrow}=170$ and $T^{\rightarrow}/T^{\leftarrow}=180$ for the maxima associated with the first and second negative orders in the right panel. Besides, notice the "inverse" unidirectional effect, i.e., when $T^{\rightarrow}\approx 0$ but $T^{\leftarrow}>0$, as observed in the left panel in Fig. 16(b) at Φ = 120°. Similar effect is observed for example in Figs. 10(a) and 10(b) at Φ>120° in the vicinity of kL = 7.8. Among others, this effect will be a subject of the future studies.

6. Conclusions

To summarize, we have demonstrated unidirectional transmission in the PC gratings with one-side echelette-type corrugations at beam-type illumination. Simulation results obtained for the plane-wave and Gaussian-beam illuminations, and the experimental results for the microwave horn antenna illumination were presented and analyzed. They indicate that the existence of the unidirectional transmission itself does not depend on the type of dispersion. In contrast, the appearance of this regime strongly depends on the dispersion features, which determine the width of the unidirectional transmission range and affect the behavior of the transmission within the neighboring ranges of the observation and incidence angles. For the studied mechanism, all the waves have linear polarization, while strong directional selectivity is obtained due to the different conditions of coupling of higher diffraction orders at the corrugated and non-corrugated interfaces. We have observed a good connection between the features detected at plane-wave, Gaussian-beam and horn antenna illuminations. For a wide Gaussian beam, all basic features of the transmission inferred from the plane-wave analysis remain, so that the ranges of the unidirectional transmission appear within nearly the same frequency bands. On the other hand, a wider angular spectrum of the incident wave and a variation in the distance from the source to the input interface lead to the transformation in the ranges of the unidirectional transmission, so that one-way and two-way transmissions can co-exist for the horn antenna illumination. The future studies will be dedicated, in particular, to the effect of the angular spectrum of the incident wave and the curvature of the incident wavefronts on the unidirectional transmission, as well as to the effect of the corrugation shape on the lateral beam shift and the possible reduction of the reflections at the unidirectional transmission.

Acknowledgments

This work is supported by the European Union under the projects PHOME, ECONAM, N4E, and TUBITAK under Project Nos., 109E301, 107A004, 107A012, and DPT under the project DPT-HAMIT. A.S. thanks the Deutsche Forschungsgemeinschaft for support of this work under Project No. SE1409.2-1. One of the authors (E.O.) acknowledges partial support from the Turkish Academy of Sciences.

#133429 - $15.00 USD Received 16 Aug 2010; revised 23 Sep 2010; accepted 27 Sep 2010; published 6 Oct 2010